

Journal of Biomedical Optics

SPIEDigitalLibrary.org/jbo

Multifunctional nanoprobe to enhance the utility of optical based imaging techniques

Yeongri Jung
Guangying Guan
Chen-wei Wei
Roberto Reif
Xiaohu Gao
Matthew O'Donnell
Ruikang K. Wang

Multifunctional nanoprobe to enhance the utility of optical based imaging techniques

Yeongri Jung, Guangying Guan, Chen-wei Wei, Roberto Reif, Xiaohu Gao, Matthew O'Donnell and Ruikang K. Wang
University of Washington, Department of Bioengineering, 3720 15th Avenue NE, Seattle, Washington 98195

Abstract. Several imaging modalities such as optical coherence tomography, photothermal, photoacoustic and magnetic resonance imaging, are sensitive to different physical properties (i.e. scattering, absorption and magnetic) that can provide contrast within biological tissues. Usually exogenous agents are designed with specific properties to provide contrast for these imaging methods. In nano-biotechnology there is a need to combine several of these properties into a single contrast agent. This multifunctional contrast agent can then be used by various imaging techniques simultaneously or can be used to develop new imaging modalities. We reported and characterized a multifunctional nanoparticle, made from gold nanoshells, which exhibits scattering, photothermal, photoacoustic, and magnetic properties. © 2012 Society of Photo-Optical Instrumentation Engineers (SPIE). [DOI: 10.1117/1.JBO.17.1.016015]

Keywords: gold-coated magnetic silica nanoparticle; multifunctional contrast agent; scattering-based optical coherence tomography; photothermal optical coherence tomography; magnetomotive photoacoustic imaging.

Paper 11488 received Sep. 7, 2011; revised manuscript received Nov. 28, 2011; accepted for publication Dec. 2, 2011; published online Jan. 31, 2012.

1 Introduction

Several contrast agents have been developed to enhance the quality of current imaging modalities, such as ultrasound and nuclear magnetic resonance imaging.^{1,2} Recent advances in nanotechnology have enabled the development of various nano-sized contrast agents for applications in many research areas such as diagnosis and therapy as well as the development of innovative imaging techniques.³ The physical and structural properties of these agents can be customized to enhance the signal-to-noise ratio (SNR) of the imaging modalities they have been developed for. For example, quantum dots with uniform size and fluorescence properties have been developed for the study of intercellular and/or intracellular processes at the single-molecular level.⁴ Unfortunately, these agents present potential human toxicity and cytotoxicity due to the semiconductor materials from which they are made; this is a significant limitation for *in vivo* biological applications.

Gold nanoparticles have become an attractive imaging contrast agent because they present low toxicity and can be synthesized for immuno-targeting. Recently, the light scattering properties of gold nanoparticles have been used with scattering-based optical modalities, such as optical coherence tomography (OCT), to enable high resolution imaging for early cancer detection.^{5,6} However, the improvements are limited by the low SNR due to the high scattering background of biological tissues.

To overcome limitations from the intrinsic scattering background, optical absorption based imaging modalities such as photoacoustic (PA) and photothermal (PT) imaging have been developed. PA and PT imaging do not rely on ballistic photon excitation and combine the advantage of optical absorption as a primary contrast with high spatial resolution.^{7,8}

Recently, gold-based contrast agents have been used to significantly improve both spatial resolution and imaging contrast for both of these modalities.^{8,9}

Gold nanoparticles can be easily customized to absorb light within the near-infrared (NIR) region, an attractive spectral window that presents low absorption in biological tissues enabling deeper light penetration. Also, gold nanoparticles exhibit PT (converts light into heat) and PA (converts light to sound) properties, which have been used for both diagnosis and treatment (i.e. photothermal therapy) of several diseases.³

Similarly, magnetic nanoparticles (MNP) have been designed for diagnosis and therapy in magnetic resonance imaging (MRI).^{2,10} Their most unique feature is the ability to react to a magnetic force, which has been utilized for a number of bio-applications.¹¹ MRI provides high tissue penetration; however, it presents low spatial resolution and molecular sensitivity, which limits its applicability for molecular imaging. On the other hand, optical imaging techniques generally have higher spatial resolution and molecular sensitivity, but with a tissue penetration depth limited to a few millimeters. A contrast agent with multifunctional properties can enable a combination or new imaging method that takes advantage of the benefits from each imaging technique.

In this regard, Jin et al. recently developed a new class of multifunctional nanoprobe that uses iron oxide and gold-coupled core-shell nanoparticles with well-defined structural characteristics to yield magnetic and absorption properties appropriate for MRI and photoacoustic imaging.¹² However, the size of the synthesized nanoparticles is in the order of ~30 nm, difficult to be used as a contrast agent to enhance the ability of scattering-based optical imaging techniques. In this paper, we report the synthesis of gold-coated magnetic silica nanoparticle (GMSNP) that exhibits coupled magnetic, scattering, and NIR absorption properties. We then focus on the

Address all correspondence to: Ruikang K. Wang, Department of Bioengineering, University of Washington, 3720 15th Avenue NE, Seattle, Washington 98195. Tel: 206 616 5025; Fax: 206 685 3300, E-mail: wangrk@u.washington.edu

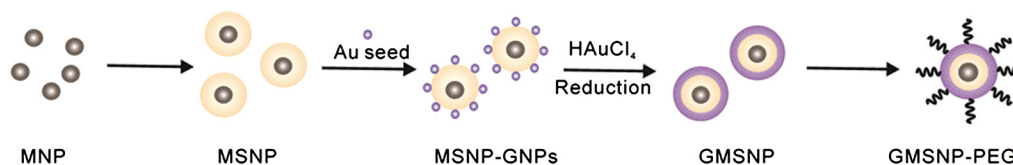


Fig. 1 Schematic illustration of GMSNP synthesis. (Color online only.)

potential use of these synthesized, multifunctional nanoparticles to enhance the utility of scattering-based optical coherence tomography (OCT), photothermal OCT, and magnetomotive photoacoustic (mmPA) imaging techniques.

2 Preparation and Methods

2.1 Multifunctional Nanoprobe Synthesis

Figure 1 schematically steps through multifunctional magnetic gold nanoshell preparation. First, the MNPs were prepared by thermal composition as previously described,¹³ onto which the magnetic silica nanoparticles (MSNP) were prepared through the water-in-oil micro-emulsion technique using tetraethyl orthosilicate (TEOS). In doing so, pre-dissolved magnetic nanocrystals in cyclohexane (2 mg mL^{-1}) were injected into a pre-dissolved surfactant of 8 mL Igepal CO 520 in 200 mL cyclohexane. In this case, the concentration of MNP dissolved in cyclohexane was varied from 0.4 to 2 mg mL^{-1} , which would make desired silica shells with a thickness ranging from 7 to 12 nm. Then, 1.3 mL of 30% NH_4OH solution was added drop by drop and vigorously stirred for 10 min with an additional 3 mL TEOS. The mixed solution was stirred for 15 h at room temperature and then was washed with ethanol and centrifuged five times to produce MSNP.

The surface of the resultant MSNP (0.4 g) was functionalized with amine groups by treating with 3-aminopropyltrimethoxysilane (75 μL) in refluxing ethanol (50 mL) for 3 h. Subsequently, the MSNPs were purified by centrifuging and dispersed in water. A gold seed solution of 2 to 3 nm was prepared to synthesize the gold-nanoparticle attached MSNP (MSNP-GNP) according to the protocol reported.¹⁴ Briefly, 0.5 mL of 1M NaOH and 1 mL tetrakis(hydroxymethyl) phosphonium chloride (THPC, prepared by adding 12 μL of 80% THPC in water to 1 mL deionized water) were added into 45 mL water, and then the mixture was stirred for 5 min. 2 mL of 1 wt.% HAuCl_4 was added quickly to the stirred solution. Next, 10 mg of amine functionalized MSNP in 5 mL ethanol were stirred with freshly prepared 2 to 3 nm sized gold seed solution for 2 h. The resulted solution was centrifuged and dispersed in 1 mL water, resulting in MSNP-GNP ready for use.

The following steps were used to grow gold nanoshells onto the MSNP-GNPs. First, 25 mg potassium carbonate in 100 mL water was mixed with 2 mL of 1 wt.% HAuCl_4 . In this way, the color of the mixed solution would change from yellow to colorless. At this step, while vigorously stirring the solution, we added 200 μL of the MSNP-GNPs into 5 mL of the colorless solution, the color of which changed from colorless to blue, meaning that the GMSNP was formed. Then, the GMSNPs were centrifuged and re-dispersed them 1 mL water. For ultimate in vivo imaging applications, polyethylene glycol with

attached thiol group (mPEG-SH) can be conjugated with the GMSNP so that it is biocompatible.

Note that apart from the GMSNP, all nanoparticles resulting from intermediate steps above are readily available for different imaging purposes by utilizing their unique optical properties.

2.2 Nanoparticle Characterization

To characterize the morphology and size of the particles, we used transmission electron microscopy (TEM). The extinction coefficient was obtained by placing solutions in a spectrophotometer (TECAN, i-580), which covers ultraviolet, visible and near-infrared regions of the optical spectrum from 400 to 1000 nm.

To determine photothermal properties of the particles, 16 solid phantoms were prepared with agarose and milk (1 $\mu\text{L}/1 \text{ mL}$). Milk was used to mimic the background scattering properties found in biological tissues. One phantom was used as the control (milk only), while the other 12 phantoms contained MSNP, MSNP-GNP or GMSNP at concentrations of 0.5, 1.0, 1.5, 2.0 or 2.5 nM.

To observe the photothermal properties of the particles, we used a spectral domain photothermal optical coherence tomography (PT-OCT) system, which has been previously described.¹⁵ The experimental system is illustrated in Fig. 2. A superluminescent diode (SLD) with a central wavelength of 1310 nm and a bandwidth of 56 nm was used as an OCT light source, providing an axial resolution of $\sim 13 \mu\text{m}$ (SLD). The diode output was split into two beams (reference and sample arm) via a beam splitter. Light in the reference arm was reflected from a stationary mirror. A pump laser beam with a wavelength of 808 nm was used to photothermally excite the nanoprobe (maximum absorption peak of $\sim 790 \text{ nm}$). The pump laser was modulated at

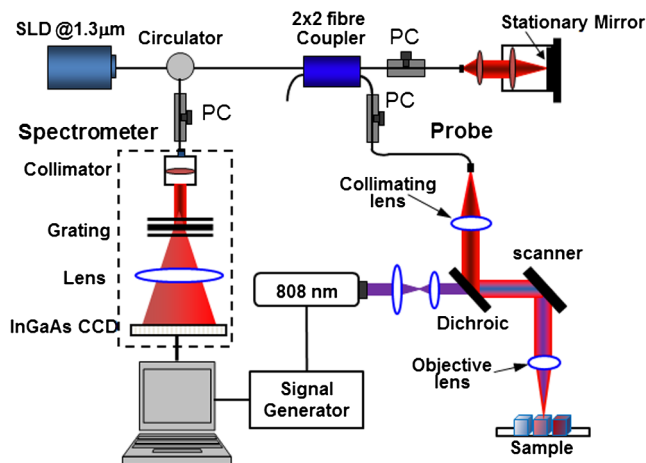


Fig. 2 Schematic illustration of photothermal OCT for imaging GMSNP. (Color online only.)

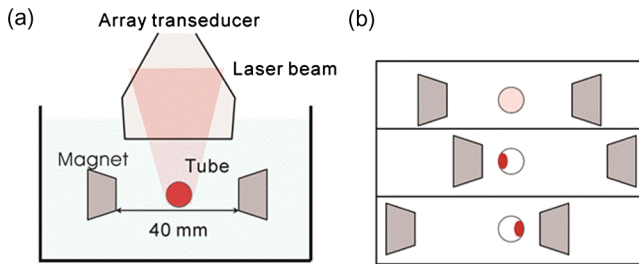


Fig. 3 (a) Experimental setup of the mmPA imaging system. (b) Translation of the magnet system for dynamic magnetic manipulation of GMSNP. (Color online only.)

400 Hz with a function generator, producing an average optical power of $\sim 0.125 \text{ mJ/cm}^2$.

Light from the SLD and the pump laser were combined in the sample arm with a dichroic mirror, and focused into the sample with an achromatic objective lens with a focal length of 50 mm. The size of the focal spot on the sample was $\sim 120 \mu\text{m}$ and $\sim 20 \mu\text{m}$ for the 808 and 1310 nm light sources, respectively. A 2×2 optical fiber coupler was used to recombine the light backscattered from the sample and reflected from the reference mirror. The combined light was re-routed with the optical circulator towards a spectrometer, consisting of a 100 mm focal length collimator, a 1200 lines/mm transmitting grating, an achromatic lens with a 50 mm focal length, and a 14 bit, 1024 pixels InGaAs line scan camera with a maximum acquisition rate of 47 kHz. This spectrometer setup had a spectral resolution of 0.055 nm, which gave a maximum imaging depth of $\sim 3.0 \text{ mm}$. A personal computer was used to synchronously control the acquisition of the camera and the square wave excitation of the pump laser. 1000-line M-mode acquisition was performed at each transverse position with an acquisition rate of 2238 Hz.

To determine the photothermal effect, nanoparticles were excited with the 808 nm light source. The absorbed light increases the temperature of the nanoparticles, leading to a change in the optical pathlength of the tissue where the absorber

is localized. Optical pathlength changes were detected by measuring phase changes in the OCT signals using the PT-OCT system. The detailed data processing methods have been previously described.¹⁵ PT-OCT images were obtained from each phantom.

Finally, to demonstrate the magnetic properties of GMSNP, we used a mmPA imaging system. The mmPA system includes a pair of magnets to physically move the particles and a photoacoustic imaging system to detect the location of the particles. The setup for mmPA imaging is shown in Fig. 3(a). A solution of 0.5 nM GMSNP was placed within a translucent Polytetrafluoroethylene (PTFE) tube (SLTT-16-72, Zeus, SC) with a diameter of 1.6 mm. Two magnets, separated by 40 mm, were placed on the left and right sides of the tube to produce a magnetic field of 0.5 Tesla in the tube region, as illustrated in the upper row in Fig. 3(b). The center of the two magnets was moved left [shown in middle row in Fig. 3(b)] and right [bottom row in Fig. 3(b)] with respect to the tube, thereby applying different magnetic forces on the particles inside the tube. This force physically moves GMSNP towards the magnet closer to the tube.

For PA signal generation, laser pulses from a tunable laser (Surelite OPO plus, Continuum, CA) operating at 730 nm, corresponding to the peak absorption wavelength of the nanoprobe, were delivered to the tube with a tilt angle of about 45 degrees to the vertical line. The laser fluence was $\sim 5 \text{ mJ/cm}^2$. A linear ultrasound transducer array (AT8L12-5 50 mm, Broad-sound, Taiwan) interfaced with an imaging system (Verasonics, WA) was used to detect and acquire the excited acoustic waves from the top of the tube. The tube, the magnets, and the transducer were immersed in a water tank to facilitate propagation of the generated acoustic waves. The frame rate of the acquisition system was 2 Hz, fast enough to observe manipulation of the nanoprobe by a magnetic force.

3 Results and Discussion

Figure 4(a) illustrates the multifunctional properties of the nanoprobe. The gold shell's physical properties are similar to gold colloids and exhibit high scattering and absorption

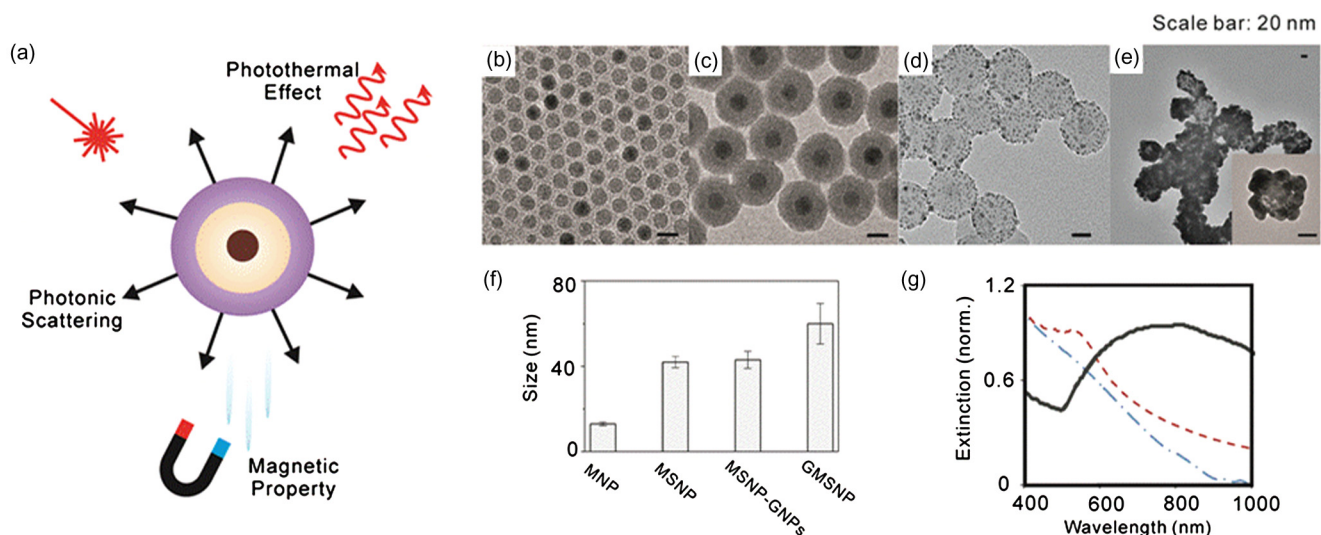


Fig. 4 (a) Illustration of the multifunctional properties of GMSNP as a contrast agent for optical imaging techniques. Transmission electron microscopy images of (b) MNP, (c) MSNP, (d) MSNP-GNRs (e) GMSNP. (f) The size distribution of each nanoparticle. (g) UV-Vis-NIR extinction of MNP, MSNP and GMSNP. The characteristic absorbance of GMSNP is red-shifted due to the outer gold shell. (Color online only.)

properties due to the strong plasmon resonance of the metallic, dielectric, concentric, and spherical configuration.¹⁶ To illustrate the multifunctionality of the nanoprobe as a contrast agent for optical imaging techniques, we tested their physical and characteristic properties including size, extinction spectrum, photothermal and magnetic properties. Using TEM, we were able to determine the diameter of the particles at different stages of synthesis. Figures 4(b)–4(e) present TEM images of MNP, MSNP, MSNP-GNPs and GMSNP, respectively, and Fig. 4(f) shows the average and standard deviation of particle diameters. The spectral extinction at different stages of nanoprobe development is presented in Fig. 4(g). The maximum absorbance (λ_{\max}) of the GNPs as seeds is at 520 nm; however, λ_{\max} of GMSNP is red-shifted to 800 nm due to the formation of a gold nanoshell on the silica surface. The peak of the extinction can be tuned by varying the core size and shell thickness.¹⁶ Ideally, the desired absorption peak should be located within the NIR region where the optical penetration depth in biological tissue is high due to low absorption.

Figures 5(a) and 5(b) show scattering and photothermal OCT images obtained from a control phantom and phantoms with 5 nM MSNP, MSNP-GNP, and GMSNP. Qualitatively, we can observe that the signal of the GMSNP phantom is higher compared to the others. Figure 5(c) shows an example of the OCT axial intensity (A-scan) obtained from the middle point of the control phantom and the GMSNP phantom. The slope of the GMSNP phantom is higher than the control, an indication of higher attenuation coefficient.¹⁷ The MSNP and MSNP-GNP had a similar curve as the control phantom (data not shown).

To test the efficacy of GMSNP as a photothermal contrast agent, we obtained PT-OCT images. The phantoms were excited with an 808 nm laser. Figure 5(b) shows a B-scan photothermal OCT image of the phantom before and after gold nanoshells are delivered at a concentration of 5.0 nM. Compared with non-absorbing nanoparticles, GMSNP was the only particle with a photothermal signal due to its strong surface plasmon resonance from the outer gold nanoshell. Figure 5(d) shows photothermal images at concentrations of 0.5, 1.0, 1.5, 2.0, and 2.5 nM. The PT signal increases with increased GMSNP concentration. Figure 5(e) shows the photothermal signal obtained from the center point of each phantom. As expected, the photothermal signal is nearly linear with the concentration of GMSNP. It is important to note that the photothermal properties could also be used for phototherapeutic applications.

The sensitivity of GMSNP on photothermal OCT is 0.5 nM, for an illumination power of 0.125 mJ/cm². The sensitivity would increase proportionally with an increase in the laser power. It has been demonstrated that with a power of 2.5 mJ/cm², photothermal OCT can be sensitive to 2 pM gold nanorods.¹⁵

To show the magnetic properties of GMSNP, we first used a simple experimental setup in which a magnet was used to apply magnetic force to GMSNP dispersed in solution. Figures 6(a) and 6(b) show a solution of 0.5 nM GMSNP without and with a magnetic field applied, respectively. The solution is dark when GMSNP is homogeneously distributed within the solution; however, when a magnetic field is applied, the solution becomes transparent because particles accumulate on the side of the container where the magnet is located, demonstrating that GMSNP exhibits magnetic properties.

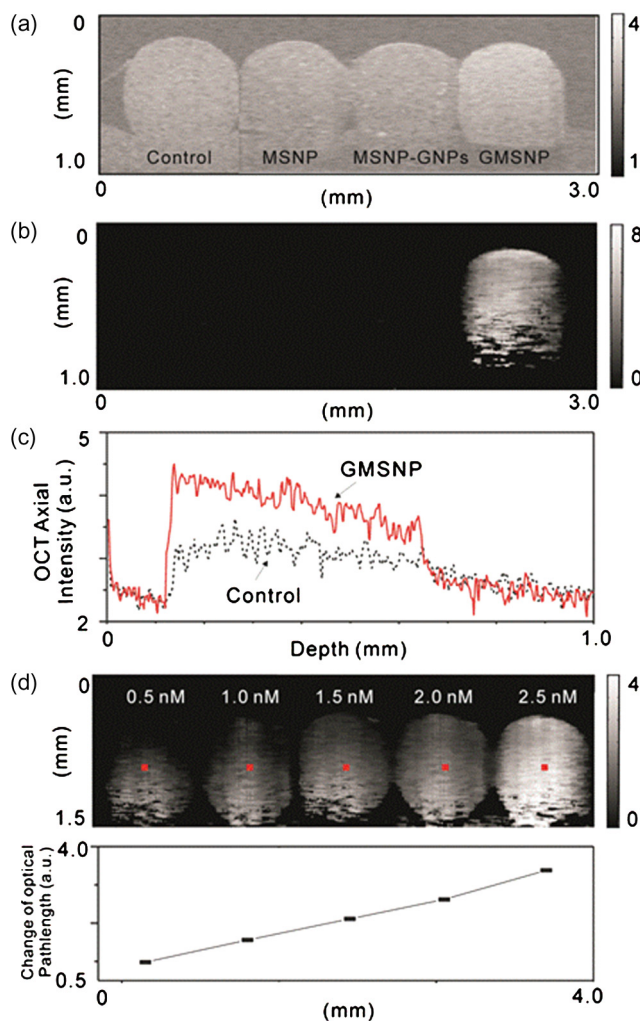


Fig. 5 (a) Conventional scattering and (b) photothermal OCT images of control, MSNP, MSNP-GNPs and GMSNP at a concentration of 5.0 nM. (c) depth-dependent OCT intensity decay of control and 5.0 nM GMSNP. (d) At different concentrations of GMSNP, photothermal images show distinguishable contrast, even though the concentration increases over a small range (left: 0.5 nM, middle: 1.5 nM, Right: 2.5 nM). (e) Plot of photothermal signal strength at the center of each phantom in (d). (Color online only.)

GMSNP with coupled photoacoustic and magnetic properties was demonstrated with mmPA imaging. Figure 6(c) shows photoacoustic images from GMSNP when the particles have been exposed for 1 h to a magnetic field peaked on the left (left image) versus exposure for the same period to a magnetic field peaked on the right [right image—see Fig. 3(b)]. The nanoparticles clearly follow the location of the magnetic force. Figure 6(d) presents the accumulation curves as a function of time for the left and right side magnet location, respectively. They were obtained by averaging the mean intensity value of the PA signal within a 0.5 mm × 0.5 mm rectangular region in each image frame, as depicted by the dashed rectangle in Fig. 6(c). It takes ~25 min for accumulation to reach saturation. Finally, the center of the magnets was dynamically oscillated left and right, as shown in Fig. 6(f). The PA images illustrate GMSNP movement as a function of time in Fig. 6(e). Consequently, coherent motion processing of PA images can be directly related to GMSNP movement. Although MNP and

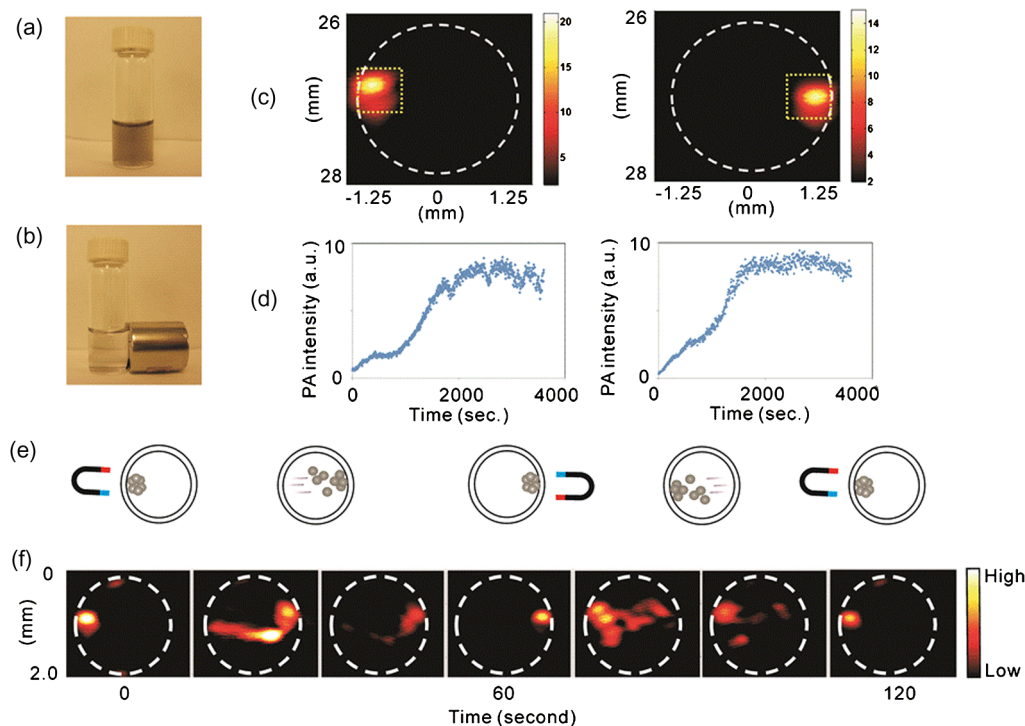


Fig. 6 Photograph of GMSNP (a) without and (b) with a magnetic field applied. (c) PA images of accumulated GMSNP when left (left)/right (right) magnet is closer to the tube. (d) Mean PA intensity versus time of accumulated GMSNP obtained by computing the mean value within the left and right rectangular region in (c). The rectangular region is $0.5 \times 0.5 \text{ mm}^2$ (vertical \times horizontal). (e), (f) Dynamic manipulation of accumulated GMSNP by changing the positions of the magnets left and right. (Color online only.)

MSNP have magnetic properties and can also be modulated by the magnets, they do not have high NIR absorption that would allow them to be detected with a PA imaging system. Similarly, gold based NIR contrast agents, nanorods and nanocages, can be detected with a PA imaging system; however, they do not have magnetic properties enabling magnetic manipulation. The mmPA sensitivity to GMSNPs was 5 pM when an optical power of $\sim 5 \text{ mJ/cm}^2$ was used.

4 Conclusion

We have demonstrated the synthesis of a nanoprobe with combined optical, photothermal, photoacoustic and magnetic properties. This multifunctional nanoprobe is small enough ($\sim 65 \text{ nm}$) that it may be used for single molecular imaging within cells. It has attenuation properties that can enhance the contrast of systems, such as OCT, and also has photothermal and photoacoustic properties which can be used as a contrast agent for PT-OCT and PA imaging methods. Finally, we demonstrated their magnetic properties using mmPA imaging. We expect these particles to have applications for several imaging modalities such as MRI, PA and PT-OCT, and integrated diagnostic/therapeutic techniques. An application for this multimodal particles may incorporate the aid of a catheter, which will enable OCT to image the same deep tissue structures as MRI; therefore, allowing the system to use multimodal imaging techniques over the same tissue sample.

Acknowledgments

This work was supported in part by research grants from the National Institutes of Health (R01 HL093140, R01 HL093140S, R01 EB009682 and R01 DC010201), the American

Heart Association (0855733G), and the Life Sciences Discovery Fund of the State of Washington (3292512). The content is solely the responsibility of the authors and does not necessarily represent the official views of grant giving bodies.

References

1. B. B. Goldberg, J.B Liu, and F. Forsberg, "Ultrasound contrast agents: a review," *Ultrasound Med. Biol.* **20**(4), 319–333 (1994).
2. V. Runge et al, "Paramagnetic agents for contrast-enhanced NMR imaging: a review," *Am. J. Roentgenol.* **141**(6), 1209–1215 (1983).
3. I. Brigger, C. Dubernet, and P. Couvreur, "Nanoparticles in cancer therapy and diagnosis," *Adv. Drug Deliv. Rev.* **54**(5), 631–651 (2002).
4. X. Michalet et al, "Quantum dots for live cells, in vivo imaging, and diagnostics," *Science* **307**(5709), 538–544 (2005).
5. E. V. Zagaynova et al, "Contrasting properties of gold nanoparticles for optical coherence tomography: phantom, in vivo studies and Monte Carlo simulation," *Phys. Med. Biol.* **53**(18), 4995–5009 (2008).
6. J. Chen et al, "Gold nanocages: bioconjugation and their potential use as optical imaging contrast agents," *Nano Lett.* **5**(3), 473–477 (2005).
7. M. Xu and L. V. Wang, "Photoacoustic imaging in biomedicine," *Rev. Sci. Instrum.* **77**(4), 041101–041122 (2006).
8. D. C. Adler et al, "Photothermal detection of gold nanoparticles using phase-sensitive optical coherence tomography," *Opt. Express* **16**(7), 4376–4393 (2008).
9. K. H. Song et al, "Near-infrared gold nanocages as a new class of tracers for photoacoustic sentinel lymph node mapping on a rat model," *Nano Lett.* **9**(1), 183–188 (2008).
10. I. Hilger, R. Hergt, and W. A. Kaiser, "Use of magnetic nanoparticle heating in the treatment of breast cancer," *IEE Proc. Nanobiotechnol.* **152**(1), 33–39 (2005).
11. A. H. Lu, E. L. Salabas, and F. Schüth, "Magnetic nanoparticles: synthesis, protection, functionalization, and application," *Angew. Chem. Int. Ed.* **46**(8), 1222–1244 (2007).
12. Y. Jin et al, "Multifunctional nanoparticles as coupled contrast agents," *Nat. Commun.* **1**(41), 1–8 (2010).

13. J. Park et al, "Ultra-large-scale syntheses of monodisperse nanocrystals," *Nat. Mater.* **3**, 891–895 (2004).
14. L. M. Liz-Marzán, M. Giersig, and P. Mulvaney, "Synthesis of nano-sized gold-silica core-shell Particles," *Langmuir* **12**(18), 4329–4335 (1996).
15. Y. Jung et al, "Three-dimensional high-resolution imaging of gold nanorods uptake in sentinel lymph nodes," *Nano Lett.* **11**(7), 2938–2943 (2011).
16. S. J. Oldenburg et al., "Nanoengineering of optical resonances," *Chem. Phys. Lett.* **288**(2), 243–247 (1998).
17. F. J. van der Meer et al., "Localized measurement of optical attenuation coefficients of atherosclerotic plaque constituents by quantitative optical coherence tomography," *IEEE Trans. Med. Imag.* **24**(10), 1369–1376 (2005).